https://doi.org/10.5194/egusphere-2025-3703
Preprint. Discussion started: 18 August 2025

Conditions for Instability in the Climate-Carbon Cycle System

Joseph Clarke[1,2], Chris Huntingford[3], Paul D. L. Ritchie[1,2], Rebecca Varney[1,4], Mark Williamson[1,2], and Peter Cox[1,2]

[1]Department of Mathematics and Statistics, Faculty of Environment, Science and Economy, University of Exeter, Exeter, Devon, EX4 4QF, UK
[2]Global Systems Institute, University of Exeter, Devon, Exeter, EX4 4QE, UK
[3]UK Centre for Ecology and Hydrology, Wallingford, Oxfordshire, OX10 8BB, UK
[4]Department of Physical Geography and Bolin Centre for Climate Research, Stockholm University, Stockholm, Sweden

Correspondence: Joseph Clarke (j.j.clarke@exeter.ac.uk)

Abstract. The climate and carbon cycle interact in multiple ways. An increase in carbon dioxide in the atmosphere warms the climate through the greenhouse effect, but also leads to uptake of CO_2 by the land and ocean sink, a negative feedback. However, the warming associated with a CO_2 increase is also expected to suppress carbon uptake, a positive feedback. This study addresses the question: 'under what circumstances could the climate-carbon cycle system become unstable?' It uses both a reduced form model of the climate-carbon cycle system as well as the complex land model JULES, combined with linear stability theory, to show that: (i) the key destabilising loop involves the increase in soil respiration with temperature; (ii) the climate-carbon system can become unstable if either the climate sensitivity to CO_2 or the sensitivity of soil respiration to temperature is large, and (iii) the climate-carbon system is stabilized by land and ocean carbon sinks that increase with atmospheric CO_2, with CO_2-fertilization of plant photosynthesis playing a key role. For central estimates of key parameters, the critical equilibrium climate sensitivity (ECS) that would lead to instability at current atmospheric CO_2 lies between about 11K (for large CO_2 fertilization) and 6K (for no CO_2 fertilization). The latter value is close to the highest ECS values amongst the latest Earth Systems Models. Contrary to a previous study that did not include an interactive ocean carbon cycle sink, we find that the stability of the climate-carbon system increases with atmospheric CO_2, such that the glacial CO_2 concentration of 190ppmv would be unstable even for ECS greater than around 4.5K in the absence of CO_2 fertilization of land photosynthesis.

1 Introduction

Earth's climate and carbon cycle are intimately coupled. Variations in global mean temperature throughout Earth's history have been linked to changes in atmospheric CO_2 concentrations (Zachos et al., 2001; Judd et al., 2024). The glacial-interglacial cycles that have occurred over the last 800,000 years are associated with ice-sheet dynamics and Milankovitch orbital forcing, but changes in CO_2 concentration have also played a role in significantly amplifying the glacial to interglacial differences (Petit et al., 1999; Marcott et al., 2014).

Since the mid-nineteenth century atmospheric CO_2 concentrations have increased by 50% due to anthropogenic emissions from fossil fuel burning and deforestation, which has driven global warming through an enhanced greenhouse effect (Chen

https://doi.org/10.5194/egusphere-2025-3703
Preprint. Discussion started: 18 August 2025

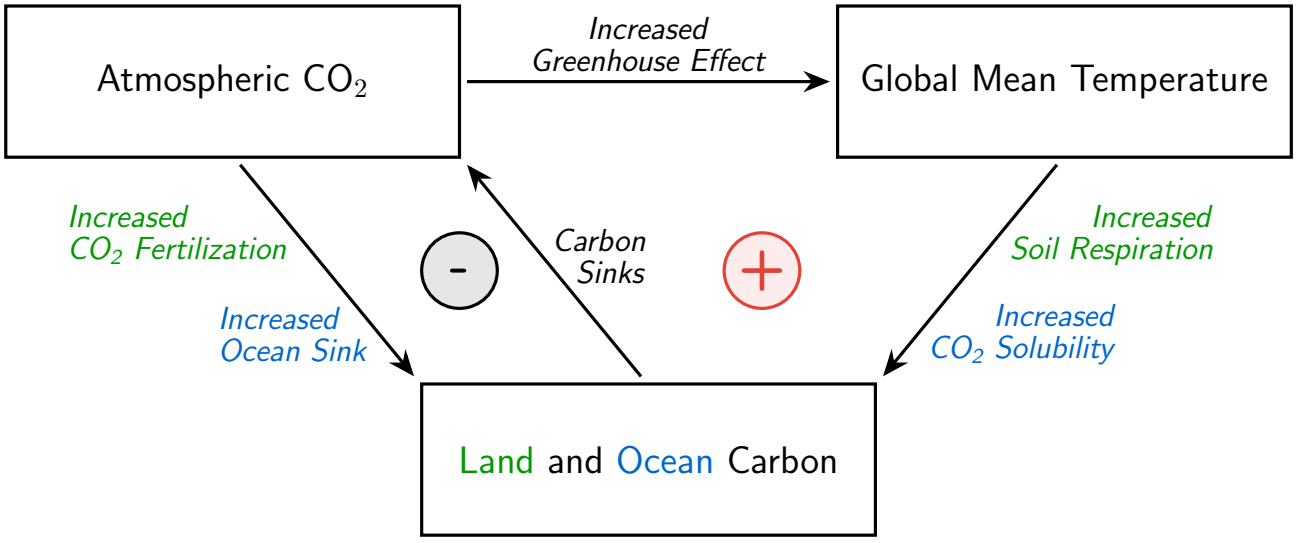

Figure 1. A schematic of the climate-carbon cycle interactions and feedbacks relevant to this study. This shows the negative (stabilising) increased CO_2 leading to increased carbon sink feedback loop, and the positive (destabilising) increased global temperatures leading to a reduced carbon sink feedback loop.

et al., 2021). Even here the carbon cycle still plays an important role, absorbing about half of the anthropogenic emissions of CO_2 through land and ocean carbon sinks (Canadell et al., 2021).

Contemporary land and ocean carbon sinks are the net effect of positive (amplifying) and negative (dampening) feedback loops (see Fig. 1). Increases in atmospheric CO_2 lead to an imbalance between the atmosphere and the surface ocean which results in additional CO_2 being dissolved in seawater and ultimately exported to depth by ocean circulations and marine biota (DeVries, 2022). In the absence of major nutrient limitations, the extra atmospheric CO_2 also increases the photosynthetic rates of land plants, which enables them to store more carbon and create the land carbon sink (Schimel et al., 2015). Both of these effects lead to an increased carbon sink due to increased CO_2. Therefore, they act to dampen an initial CO_2 perturbation (i.e. they are negative feedbacks).

The radiative forcing due to CO_2 leads to increases in global temperatures, which cause predominantly amplifying feedbacks (i.e. positive feedbacks). The positive feedbacks are particularly apparent on the land where the rate of heterotrophic respiration from the soil is known to increase significantly with warming (Davidson and Janssens, 2006; Jenkinson et al., 1991). Enhanced respiration on the land due to CO_2-induced warming is therefore projected to counteract CO_2-fertilization (Friedlingstein et al., 2006, 2014; Arora et al., 2020). In one early model, this increased temperatures leading to a reduced sink effect eventually overwhelmed CO_2 fertilisation of photosynthesis in the mid-21st century, converting the global land carbon sink into a source and significantly accelerating climate change (Cox et al., 2000).

This latter result amounted to a net positive feedback of the carbon cycle on anthropogenic climate change (feedback gain factor, $g > 0$), but it did not lead to an instability or 'runaway' (which requires $g > 1$). A subsequent analysis explored the

https://doi.org/10.5194/egusphere-2025-3703
Preprint. Discussion started: 18 August 2025

conditions that could have led to a runaway climate-carbon cycle feedback (Cox et al., 2006), concluding that this would require at least one of the Equilibrium Climate Sensitivity (ECS) or sensitivity of soil respiration to temperature to be unrealistically high, and that the climate-carbon cycle would become less stable with increases in the CO_2 concentration due to the saturation of CO_2 fertilization at high-CO_2.

In this study we reconsider the potential instability of the coupled climate-carbon system, for two main reasons. Firstly, we note that the upper range of ECS values has increased significantly in the CMIP6 generation of ESMs, with some models now recording ECS values of up to 6K (Zelinka et al., 2020). This increases the probability that some ESMs could suffer a climate-carbon cycle instability. Secondly, the Cox et al. (2006) study did not include the important stabilising effect of an interactive ocean carbon cycle, instead assuming that a fixed fraction of any atmospheric CO_2 perturbation would be taken up instantaneously by the ocean.

We use a more sophisticated representation of the ocean carbon cycle, alongside more complete representations of global warming and land carbon feedbacks, to answer the question: 'under what circumstances could the climate-carbon cycle system become unstable?'. To do this we perform a bifurcation analysis of a conceptual model of the climate-carbon system and and find our results are consistent with the output of the complex JULES global land-surface model (Clark et al., 2011; Best et al., 2011).

2 Conceptual Model

To investigate the stability of the carbon-climate system, we construct a low dimensional model which represents important climate-carbon processes. This model can be analysed to determine critical parameter values that lead to a bifurcation and can be easily integrated numerically across a range of parameter values to determine its stability.

The model is composed of a climate component which models global temperature and a carbon cycle component which calculates the fluxes of carbon between the atmosphere, land and ocean. Very slow carbon cycle processes such as the flux of carbon into and out of the solid Earth are neglected.

For the climate component, we use a two-box energy balance model. One box represents the globally averaged temperature of the atmosphere and upper ocean, T_1, and the other represents the globally averaged temperature of the deep ocean, T_2.

Radiative forcing due to a CO_2 increase heats the upper box, with a forcing due to each CO_2 doubling of $Q_{2\times}$ (Myhre et al., 1998). This logarithmic dependence means that each additional unit of CO_2 added to the atmosphere has a weaker effect than the previous.

The boxes exchange energy with each other, parametrised by a heat transfer coefficient κ, and respond to the radiative forcing caused by CO_2, which follows the standard logarithmic form. This type of model can be fitted to more complex Earth System Models (Cummins et al., 2020; Williamson et al., 2024) and has been shown to accurately reproduce the response to radiative forcing (Geoffroy et al., 2013).

https://doi.org/10.5194/egusphere-2025-3703
Preprint. Discussion started: 18 August 2025

The terrestrial carbon store, C_L, is modelled by the balance between globally averaged NPP, Π, and globally averaged heterotrophic respiration. We will neglect to explicitly represent vegetation dynamics on the assumption that the timescales of interest for the stability of the system are longer than typical vegetation timescales.

NPP is assumed to be a function of atmospheric CO_2 only. The temperature dependence of NPP is neglected, as the temperature response is weaker, at the global scale, than the CO_2 response (Varney et al., 2023). To model heterotrophic respiration we make the common assumption that it follows a Q_{10} response formula, in which respiration increases by a factor of Q_{10} for every 10K warming. We also assume that the relevant temperature for heterotrophic respiration is the temperature over land, which is larger than global temperatures by a factor $\beta \approx 1.3$ (Byrne and O'Gorman, 2018).

Ocean carbon uptake is represented with a two box model developed by Bolin and Eriksson (1959) and Glotter et al. (2014). The boxes represent the upper and deep ocean carbon stores C_1 and C_2 respectively. This model accounts for changes in ocean chemistry due to increased ocean carbon, but neglects the role of temperature on carbon uptake, as that effect is assumed to be smaller.

Atmospheric carbon, C_A, is required to close the model. C_A is calculated by applying conservation of mass to the total carbon in the system. Mathematically, the model can be written as:

$$c_1 \frac{\mathrm{d}T_1}{\mathrm{d}t} = -\lambda T_1 + \kappa(T_2 - T_1) + Q_{2\times} \log_2 \left(\frac{C_A}{C_A^*} \right) \tag{1a}$$

$$c_2 \frac{\mathrm{d}T_2}{\mathrm{d}t} = -\kappa(T_2 - T_1) \tag{1b}$$

$$\frac{\mathrm{d}C_L}{\mathrm{d}t} = \Pi(C_A) - \Pi(C_A^*) \frac{C_L}{C_L^*} e^{\alpha \beta T_1} \tag{1c}$$

$$\frac{\mathrm{d}C_1}{\mathrm{d}t} = \nu_1 (C_A - \mathcal{E}(C_1)) - \nu_2 \left(C_1 - \frac{V_1}{V_2} C_2 \right) \tag{1d}$$

$$\frac{\mathrm{d}C_2}{\mathrm{d}t} = \nu_2 \left(C_1 - \frac{V_1}{V_2} C_2 \right), \tag{1e}$$

with carbon conservation giving

$$C_A + C_L + C_1 + C_2 = C_A^* + C_L^* + C_1^* + C_2^*, \tag{2}$$

where asterisks indicate pre-industrial values.

The parameters c_1 and c_2 denote the different heat capacities of the two climate boxes. Furthermore, rather than working with ECS directly, we introduce a climate feedback parameter λ, which is related to ECS by the formula $\mathrm{ECS} = Q_{2\times}/\lambda$.

The parameter α determines the strength of heterotrophic respiration and is related to Q_{10} by $\alpha = 0.1 \log Q_{10}$. The exact form of Π is not important for analytical results, as the linear stability of the pre-industrial equilibrium will only depend on $\Pi(C_A^*)$ and its derivative $\Pi'(C_A^*)$. However for numerical experiments, we assume the saturating form

$$\Pi(C_A) = \Pi(C_A^*) \frac{C_A^* + C_{1/2}}{C_A^*} \frac{C_A}{C_A + C_{1/2}} \tag{3}$$

where $C_{1/2}$ is a half-saturation constant.

https://doi.org/10.5194/egusphere-2025-3703
Preprint. Discussion started: 18 August 2025

The ocean boxes absorb carbon over different timescales. The upper box, with volume V_1, absorbs carbon over a fast timescale ν_1^{-1} and the larger lower box, with volume V_2, on a slower timescale, ν_2^{-1}. We account for the effects of ocean chemistry with the function $\mathcal{E}$, which relates C_1 to the amount of atmospheric carbon required for equilibrium. The functional form of $\mathcal{E}$ can be derived by assuming constant alkalinity, Alk, in the ocean. The expression for $\mathcal{E}$ is

$$\mathcal{E}(C_1) = k\left(1 + \frac{k_1}{[\mathrm{H}^+]} + \frac{k_1 k_2}{[\mathrm{H}^+]^2}\right)^{-1} C_1 \tag{4}$$

where the concentration of hydrogen ions, $[\mathrm{H}^+]$, can be found by solving

$$Alk = \left(\frac{k_1}{[\mathrm{H}^+]} + \frac{2k_1 k_2}{[\mathrm{H}^+]^2}\right)\left(1 + \frac{k_1}{[\mathrm{H}^+]} + \frac{k_1 k_2}{[\mathrm{H}^+]^2}\right)^{-1} C_1. \tag{5}$$

The total amount of carbon in the system can be written as the sum of $C_L^*, C_1^*, C_2^*, C_A^*$ which are the pre-industrial carbon stores in the land, upper ocean, deep ocean and atmospheric reservoirs respectively. Whilst C_L^* and C_A^* are free parameters of the model, the pre-industrial ocean values are calculated from the equations $C_A^* = \mathcal{E}(C_1^*)$ and $C_1^* = (V_2/V_1)C_2^*$.

2.1 Parameters

The parameters take the values given in table 1, unless otherwise stated. These values mostly come from previous estimates in the literature, however some come from the output of a complex terrestrial carbon cycle model, JULES. The only parameter that we have fitted ourselves is the Alk parameter, which was chosen so that the ocean model correctly estimates the observed ocean carbon uptake over the historical period, inferred by the Global Carbon Budget (GCB) (Friedlingstein et al., 2022) (see supplementary Fig. S1).

2.2 Analysis

The pre-industrial state is an equilibrium of equation (1), occurring when $T_1 = T_2 = 0$, $C_A = C_A^*$, $C_L = C_L^*$, $C_1 = C_1^*$ and $C_2 = C_2^*$. Furthermore, this equilibrium exists for all parameter values.

To calculate the stability of this pre-industrial equilibrium it is helpful to rewrite equation (1) in the condensed form

$$\frac{\mathrm{d}\boldsymbol{x}}{\mathrm{d}t} = \boldsymbol{f}(\boldsymbol{x}) \tag{6}$$

where $\boldsymbol{x} = (T_1, T_2, C_L, C_1, C_2)^T$ and $\boldsymbol{f}$ is given by the right-hand side of equation (1). Letting $\boldsymbol{x}^*$ be the pre-industrial equilibrium, we can linearise equation (6) about $\boldsymbol{x}^*$ to give the behaviour of small perturbations $\boldsymbol{\Delta x}$

$$\frac{\mathrm{d}\boldsymbol{\Delta x}}{\mathrm{d}t} = \mathbf{J}\boldsymbol{\Delta x} \tag{7}$$

where the Jacobian, $\mathbf{J}$, is given by $\mathbf{J}_{ij} = \partial \boldsymbol{f}_i / \partial \boldsymbol{x}_j$ evaluated at $\boldsymbol{x}^*$.

At large t, the perturbation will be dominated by a contribution along the fastest growing (or slowest decaying) direction in phase space. Mathematically, as $t \to \infty$, the perturbation behaves like $\boldsymbol{\Delta x}(t) \sim c_m \boldsymbol{v}_m \exp(\gamma_m t)$ where γ_m is the eigenvalue of $\mathbf{J}$ with the largest real part, $\boldsymbol{v}_m$ the corresponding eigenvector and c_m a constant given by the initial conditions. If $\mathrm{Re}\,\gamma_m > 0$,

https://doi.org/10.5194/egusphere-2025-3703
Preprint. Discussion started: 18 August 2025

Parameter	Name	Value	Source
C_A^*	Pre-industrial atmospheric carbon	286.085 ppmv	JULES
C_L^*	Pre-industrial land carbon	1630 PgC	JULES
$C_{1/2}$	CO_2 fertilisation saturation constant	344 ppmv	JULES
$\Pi(C_A^*)$	Pre-industrial NPP	65 PgCyr^{-1}	JULES
Q_{10}	Respiration temperature sensitivity	2	Jones and Cox (2001)
κ	Heat transfer coefficient	0.57 $\mathrm{Wm}^{-2}\mathrm{K}^{-1}$	Williamson et al. (2024)
c_1	Upper box heat capacity	7.7 $\mathrm{Wm}^{-2}\mathrm{K}^{-1}\mathrm{yr}^{-1}$	Williamson et al. (2024)
c_2	Lower box heat capacity	100.0 $\mathrm{Wm}^{-2}\mathrm{K}^{-1}\mathrm{yr}^{-1}$	Williamson et al. (2024)
$Q_{2\times}$	Radiative forcing due to doubled CO_2	3.7 Wm^{-2}	Myhre et al. (1998)
β	Ratio of land to global warming	1.3	Byrne and O'Gorman (2018)
ν_1	Ocean carbon uptake rate	0.2 yr^{-1}	Bolin and Eriksson (1959)
ν_2	Ocean carbon uptake rate	0.002 yr^{-1}	Bolin and Eriksson (1959)
Alk	Ocean alkalinity	5130 PgC	GCB
k	Ocean/atmosphere carbon ratio	220.0	Glotter et al. (2014)
k_1	Dissociation constant	10^{-6} molkg^{-1}	Glotter et al. (2014)
k_2	Dissociation constant	7.53×10^{-10} molkg^{-1}	Glotter et al. (2014)
V_2/V_1	Ocean box volume ratio	50	Bolin and Eriksson (1959)

Table 1. The 'default' parameter values used for the numerical evaluation of the model, unless otherwise stated. No default value is given for λ as that parameter is changed throughout the study.

the perturbation grows and therefore the equilibrium is unstable. If $\mathrm{Re}\,\gamma_m < 0$ the perturbation decays and so the equilibrium is stable.

Therefore we must determine when the eigenvalues of $\mathbf{J}$ have zero real part to find the critical parameters for which the stability of the pre-industrial equilibrium changes. Evaluated at the pre-industrial equilibrium, $\mathbf{J}$ is

$$\mathbf{J} = \begin{pmatrix} -\frac{\lambda+\kappa}{c_1} & \frac{\kappa}{c_1} & -\frac{Q_{2\times}}{c_1 C_A^* \log 2} & -\frac{Q_{2\times}}{c_1 C_A^* \log 2} & -\frac{Q_{2\times}}{c_1 C_A^* \log 2} \\ \frac{\kappa}{c_2} & -\frac{\kappa}{c_2} & 0 & 0 & 0 \\ -\alpha\beta\Pi(C_A^*) & 0 & -\frac{\mathrm{d}\Pi}{\mathrm{d}C_A} - \frac{\Pi(C_A^*)}{C_L^*} & -\frac{\mathrm{d}\Pi}{\mathrm{d}C_A} & -\frac{\mathrm{d}\Pi}{\mathrm{d}C_A} \\ 0 & 0 & -\nu_1 & -\nu_1\left(1+\mathcal{E}'(C_1^*)\right) - \nu_2 & -\nu_1 + \frac{V_1}{V_2}\nu_2 \\ 0 & 0 & 0 & \nu_2 & -\frac{V_1}{V_2}\nu_2 \end{pmatrix} \tag{8}$$

where $\mathcal{E}'$ denotes the derivative of $\mathcal{E}$ with respect to C_1. The eigenvalues, γ, of the Jacobian satisfy the characteristic equation, $\det(\mathbf{J} - \gamma\mathbf{I}) = 0$ giving

$$\gamma^5 + p_4\gamma^4 + p_3\gamma^3 + p_2\gamma^2 + p_1\gamma + p_0 = 0, \tag{9}$$

https://doi.org/10.5194/egusphere-2025-3703
Preprint. Discussion started: 18 August 2025

where $\{p_i\}$ are functions of the parameters of the model.

Ideally, we would solve equation (9) for γ and would then find the critical parameter values for which $\mathrm{Re}\,\gamma = 0$. However, because equation (9) is a quintic polynomial, no general solution exists. Therefore, we must rely on special cases and approximations to make progress.

A simple case occurs when γ is purely real. In that case, $\gamma = 0$ is a solution when $p_0 = 0$. When $p_0 = 0$, The parameters satisfy

$$\frac{\alpha\beta Q_{2\times}}{\lambda \log 2} = \frac{V_2}{V_1}\frac{\mathrm{d}\log\Pi}{\mathrm{d}\log C_A} + \frac{C_A^*}{C_L^*}\left(1 + \frac{1}{\mathcal{E}'} + \frac{1}{\mathcal{E}'}\frac{V_2}{V_1}\right). \tag{10}$$

The bifurcation this corresponds to can be shown to be a transcritical bifurcation.

If γ has non-zero imaginary part, exact results cannot be obtained. However, because we are interested in γ values near the bifurcation, we can guarantee that $\mathrm{Re}\,\gamma$ is small. Making the further assumption that $\mathrm{Im}\,\gamma$ is small means that cubic terms and higher can be dropped from equation (9). The resulting quadratic equation can be solved to give

$$\mathrm{Re}\,\gamma \approx -\frac{p_1}{2p_2}, \tag{11}$$

which in terms of the climate feedback parameter, λ, can be written as

$$\mathrm{Re}\,\gamma \approx \frac{\lambda + g_1}{g_2\lambda + g_3}, \tag{12}$$

where $\{g_i\}$ are functions of the parameters.

Setting this growth rate equal to zero gives an expression for the critical λ, which is given in the supplementary material as equation S1. The resulting equation is too complicated to be useful; however further approximations can be made to make it tractable. As the deep ocean is much larger and absorbs carbon over a slower timescale than the upper ocean, it can be assumed that $\mathcal{E}'\nu_1 \gg \nu_2$, $\nu_1 \gg \nu_2$, $c_2 \gg c_1$ and $V_2 \gg V_1$. In this approximation, the equation reduces to

$$\frac{\alpha\beta Q_{2\times}}{\lambda \log 2} = \left(\frac{\mathrm{d}\log\Pi}{\mathrm{d}\log C_A} + \frac{C_A^*}{C_L^*}\left(1 + \frac{1}{\mathcal{E}'} + \frac{c_2\nu_2}{\kappa\mathcal{E}'} + \frac{C_L^*\nu_2}{\Pi_0\mathcal{E}'}\right)\right)\left(1 + \frac{C_A^*\nu_2 c_2}{C_L^*\mathcal{E}'\alpha\beta Q_{2\times}}\right). \tag{13}$$

As γ is purely imaginary, this corresponds to a Hopf bifurcation.

It should be noted that equation (10) contains factors of V_2/V_1 whereas equation (13) does not. The deep ocean is much larger than the upper ocean, $V_2 \gg V_1$. This means that the transcritical bifurcation occurs at much higher values of ECS than the Hopf bifurcation does. Therefore, we will focus on the Hopf bifurcation in the rest of the study.

The approximate expression for the critical climate sensitivity, equation (13), was verified by numerically calculating the growth rate from the Jacobian, $\mathbf{J}$, and identifying where it is zero. This numerical result was compared to equation (13) for a range of ECS and CO_2 fertilisation strengths, and for three different C_A^* values. These C_A^* values correspond to the pre-industrial equilibrium, a doubling of CO_2 and $C_A^* = 190\mathrm{ppmv}$ which was the atmospheric CO_2 level during at Last Glacial Maximum (LGM) (Kageyama et al., 2017).

The results are shown in Fig. 2. The figure shows the numerically determined growth rates, as well as the approximation equation (13). The approximation gives good agreement with the numerically determined values, supporting the usefulness of the approximation equation (13) across a range of parameter values.

https://doi.org/10.5194/egusphere-2025-3703
Preprint. Discussion started: 18 August 2025

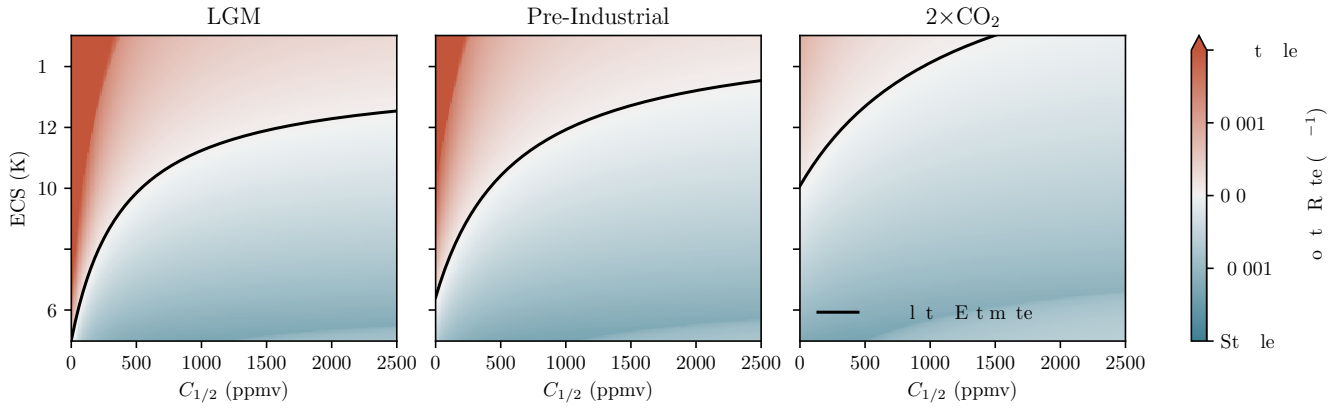

Figure 2. Growth rates of perturbations to the equilibrium state in the conceptual model, equation (1), for a range of ECS, CO_2 fertilisation effect strengths, and different atmospheric carbon levels. The colours correspond to growth rates calculated numerically and the solid line is given by equation (13). This line corresponds agrees with the numerics as to when the growth rate is zero.

It is worth dwelling on the meaning of the individual terms in equation (13). The left-hand side of the equation consists of a product of two sensitivities. One sensitivity in the product is $Q_{2\times}/\lambda = \mathrm{ECS}$, which is the sensitivity of global temperatures to atmospheric carbon. The other sensitivity is the sensitivity of respiration to increased land temperatures, $\alpha\beta$. These are the two ingredients in the positive feedback loop between global temperatures and respiration. The two factors do not enter equation (13) on totally equal terms, however, as a factor of $\alpha\beta$ also appears on the right-hand side of the equation.

The right-hand side of equation (13) consists of negative feedbacks which stabilise the climate-carbon system. The first of these is $\mathrm{d}\log\Pi/\mathrm{d}\log C_A$, which measures the magnitude of the CO_2 fertilisation effect. The larger this is, the more stable the system becomes. The next term is a factor in parentheses multiplied by the ratio C_A^*/C_L^*. This ratio implies that the greater the proportion of carbon held in the atmosphere relative to land the more stable the system is. This effect can be attributed to the fact that heterotrophic respiration increases linearly with land carbon but radiative forcing increases only logarithmically with CO_2.

The factor in parentheses is a sum of timescale ratios. The timescales are: κ/c_2 (ocean heat uptake timescale), ν_2^{-1} (deep ocean carbon uptake timescale) and C_L^*/Π_0 (soil carbon turnover time). They imply that the system is less stable if the ocean absorbs carbon slowly relative to the time the ocean takes to warm or if carbon cycles quickly through the soil compared to the ocean. Each of these timescale ratios is multiplied by $\mathcal{E}'^{-1}$, which describes how a change in ocean carbon affects the air-sea carbon equilibrium. If this value is large, the ocean absorbs more carbon for a given change in atmospheric concentration, which acts to stabilise the system.

https://doi.org/10.5194/egusphere-2025-3703
Preprint. Discussion started: 18 August 2025

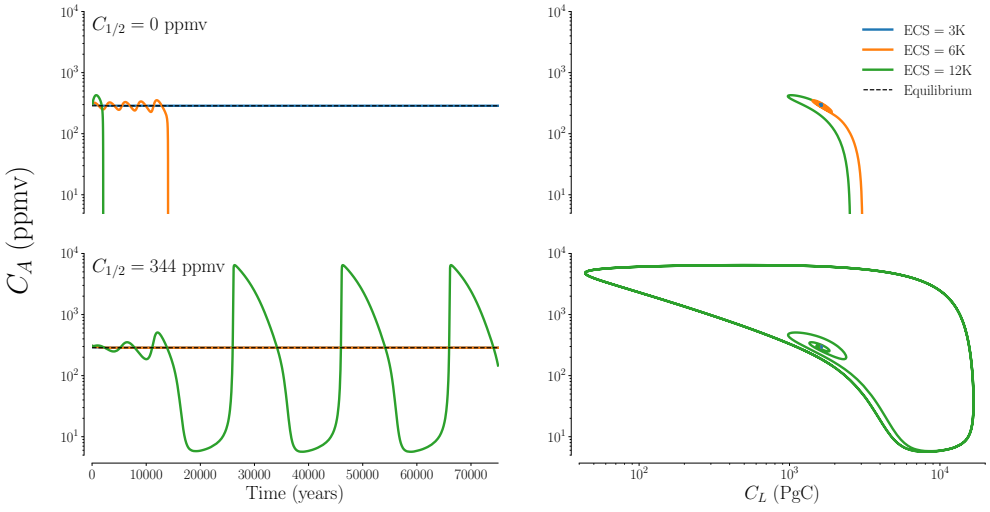

Figure 3. The response of equation (1) to a small 20ppmv perturbation to CO_2 when the ECS is 3K, 6K or 12K and the CO_2 fertilisation effect is either present or absent. The left column shows a time series of atmospheric carbon and the right shows the trajectories projected onto the C_A-C_L plane. In the top row, the CO_2 fertilisation effect is absent and in the bottom row it present.

2.3 Numerical Results

We performed numerical experiments to analyse the behaviour of the model around the bifurcation. We initialised the system near the pre-industrial equilibrium by increasing atmospheric carbon by 20ppmv and integrating for 50,000 years.

Figure 3 shows the resulting atmospheric CO_2 time series for ECS values of 3K, 6K and 12K. Additionally, we repeated the experiment in the case when the CO_2 fertilisation effect was absent. When the CO_2 effect was present, the cases where the ECS was 3K or 6K relaxed back to equilibrium; these parameters correspond to a stable equilibrium. However, for an ECS of 12K the system approaches a limit cycle. Between these ECS values the system passed through a Hopf bifurcation, causing the pre-industrial state to become unstable.

A projection of the C_A-C_L plane is shown in Fig. 3. It shows that the limit cycle involves moving large quantities of carbon between the land and the atmosphere.

The result of turning off the CO_2 fertilisation effect (i.e. setting $C_{1/2}$ to zero) is shown in the top row of Fig. 3. In this case, the pre-industrial state becomes unstable at lower values of ECS. In particular instability occurs for an ECS of 6K. Furthermore, the instability is more serious in that the system diverges rather than approaches a limit cycle. This represents a deficiency the model, arising from not accounting for effects that occur at low CO_2.

A more systematic investigation of the system's behaviour can be performed by plotting a bifurcation diagram. Figure 4 shows a bifurcation diagram of atmospheric carbon as a function of ECS for the cases with and without a CO_2 fertilisation

https://doi.org/10.5194/egusphere-2025-3703
Preprint. Discussion started: 18 August 2025

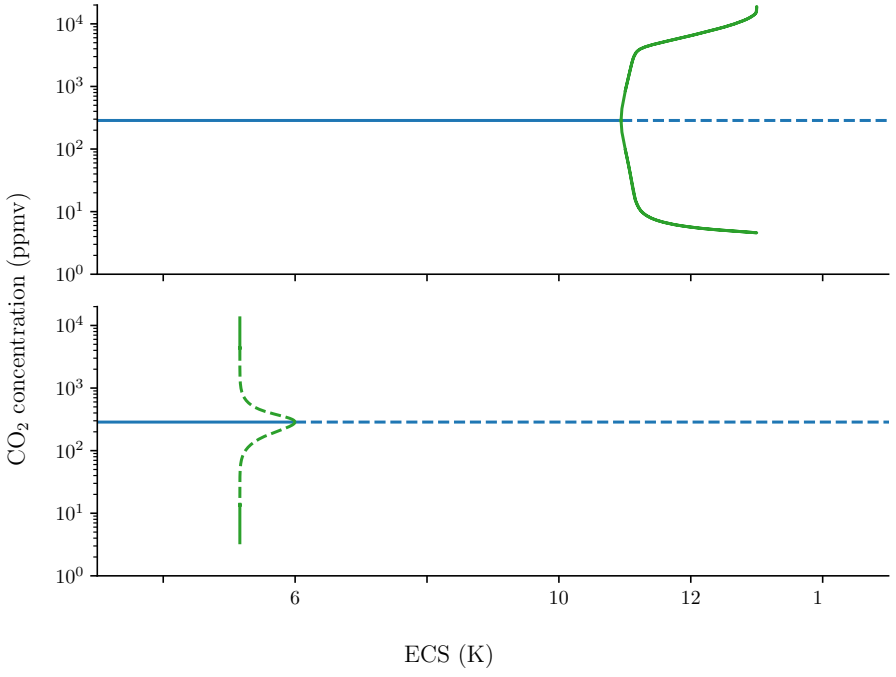

Figure 4. A bifurcation diagram for equation (1), showing the equilibrium behaviour of atmospheric carbon as a function of climate sensitivity with a CO_2 fertilisation effect (top) and without (bottom). The blue solid line indicates a stable fixed point, corresponding to the pre-industrial state. The dashed line indicates an unstable fixed point and the green curves show the maximum and minimum values of the limit cycle.

effect, computed by the XPP-AUTO continuation software (Ermentrout, 2002). Figure 4 shows that, with a CO_2 fertilisation effect, above a critical climate sensitivity of 10.9K, the pre-industrial state is unstable. Beyond this threshold, the system undergoes a supercritical Hopf bifurcation and develops large oscillations in the CO_2 levels. When the CO_2 fertilisation effect is absent, the bifurcation occurs at a lower ECS of just below 6K. Furthermore, the Hopf bifurcation is now subcritical, which explains why the system diverged in some of the numerical experiments plotted in Fig. 2.

The dependence on the CO_2 fertilisation effect strength and pre-industrial CO_2 levels were further investigated, by numerically solving for the eigenvalues of the Jacobian. Figure 5 shows the dependence of the critical ECS value on $C_{1/2}$ and C_A^* for $Q_{10} = 2$ and $Q_{10} = 3$. As C_A^* increases, the critical ECS does too. This indicates that the system is more stable at high CO_2 levels and therefore anthropogenic CO_2 emissions are unlikely to trigger this instability. Furthermore as the strength of the CO_2 fertilisation effect decreases, the system is unstable at lower ECS values.

When $Q_{10} = 2$, Fig. 5 shows that the critical ECS enters the range of CMIP6 models (i.e. less than 6K) for weak CO_2 fertilisation effects and low CO_2 levels, a regime relevant to the Last Glacial Maximum. If $Q_{10} = 3$ then the critical ECS becomes comparable to the ECS of CMIP6 models, even for a comparatively strong CO_2 fertilisation effect at low enough CO_2 levels.

https://doi.org/10.5194/egusphere-2025-3703
Preprint. Discussion started: 18 August 2025

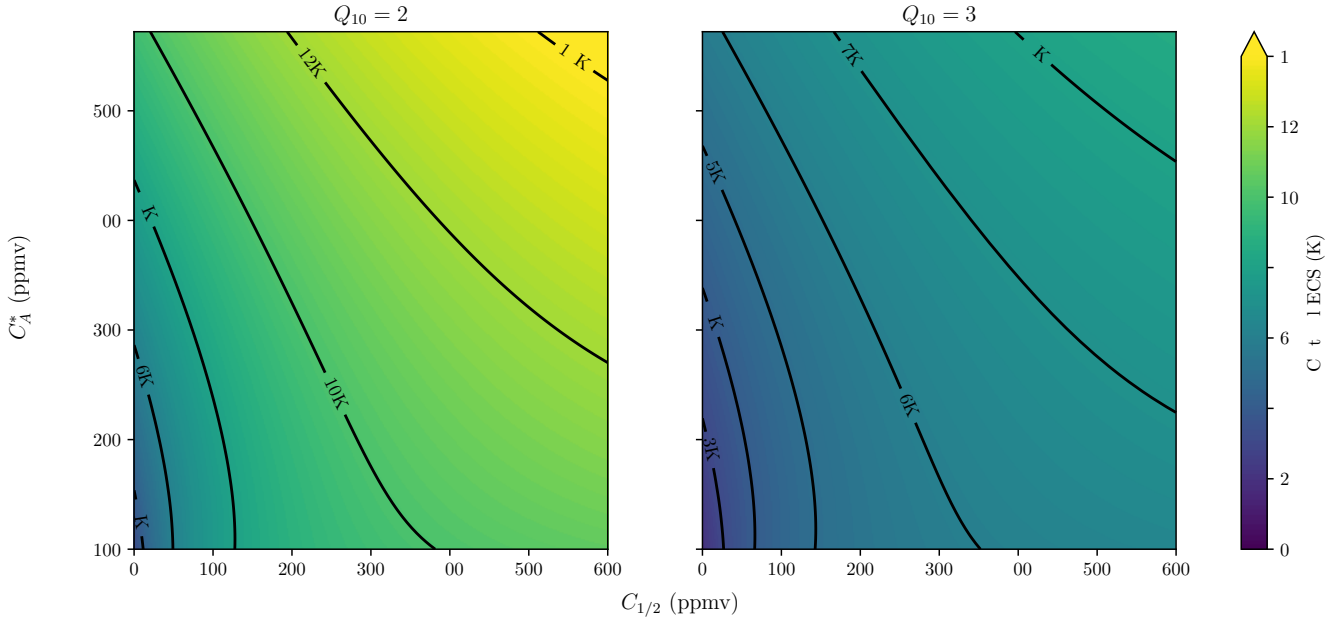

Figure 5. The critical ECS as a function of pre-industrial CO_2 levels and the CO_2 fertilisation effect for two different values of Q_{10}. Notice the critical ECS is smaller for smaller pre-industrial CO_2 levels, CO_2 fertilisation strength and larger Q_{10}.

3 Complex Model

Equation (1) is, by construction, a significant simplification of the real Earth system, which has many more processes and is spatially heterogeneous. This is important, for example, as warming caused by increased atmospheric CO_2 is also spatially heterogeneous; the poles warm faster than equatorial regions (Huntingford and Mercado, 2016). To avoid the limitations of the simple model, we examine the results from a complex land surface model, the Joint UK Land Environmental Simulator (JULES) (Best et al., 2011; Clark et al., 2011).

JULES is a state-of-the-art model of land-atmosphere exchanges of momentum, water and vapour, and fluxes of carbon. JULES has a dynamic vegetation component (TRIFFID) and a RothC four-pool model of soil carbon, operating at a spatial resolution of $2.5° \times 3.75°$. JULES is driven by meteorological forcings from a model called the Integrated Model Of Global Effects of climatic aNomalies (IMOGEN), which includes carbon cycle feedbacks on atmospheric and ocean carbon.

IMOGEN is a spatially-explicit intermediate complexity model (Huntingford et al., 2010) which is coupled to the JULES land surface model at the same spatial resolution. IMOGEN provides spatially-explicit meteorological forcings to drive JULES and dynamically responds to changes in CO_2. The response to CO_2 is estimated using pattern scaling, which assumes that the change in some spatially-resolved meteorological variable ΔX at location r, year t, and month m can be written as $\Delta X(r,t,m) = p(r,m)\overline{\Delta T}(t)$ where p is a spatial pattern and $\overline{\Delta T}$ is global mean temperature change. The temperature change

https://doi.org/10.5194/egusphere-2025-3703
Preprint. Discussion started: 18 August 2025

is determined by an energy balance model. The pattern and energy balance model parameters are fitted to the actual patterns of change projected by different ESMs. In this way, IMOGEN can emulate different ESMs (Huntingford et al., 2000). In this study, we use IMOGEN to create an emulator of the HadGEM2-ES model (Jones et al., 2011).

To close the global carbon cycle, IMOGEN also provides a model for ocean carbon uptake based on the impulse-response formulation given by Joos et al. (1996). The impulse-response function is calibrated to match the behaviour of process-based models.

For this study, we took advantage of the fact that the ECS of IMOGEN can be set explicitly. This means that we can run multiple experiments varying the ECS values to determine which value of ECS leads to an instability of the pre-industrial state.

To initialise JULES in a pre-industrial equilibrium state, the JULES/IMOGEN system was run with a prescribed constant concentration of atmospheric carbon and no ocean carbon uptake. As IMOGEN is an anomaly model, calculating changes relative to a given climatology, the equilibrium state is not a function of ECS. As a result, only one initialisation was required. JULES was run until the slowest carbon stores (namely the soil pools) reached an approximate steady state. To verify that an approximate steady state had been reached, a further 600 years of simulation was performed, and the change in soil carbon was found to be 0.008% over this period, suggesting a near-equilibrium state (also see supplementary figure S3).

Once this approximate steady state had been reached, atmospheric carbon was increased by $2\mathrm{ppmv}$ and 13 different simulations were run, each with a different ECS. In these simulations, ocean carbon uptake was enabled, and atmospheric carbon was allowed to change dynamically. The simulations lasted 5,000 years; longer integrations were ruled out due to computational limitations. After an initial transient of 250 years, the change in CO_2 was assumed to follow the form $\Delta C_A(t) \propto e^{\gamma_m t}$. A linear fit to the logarithm of this growth was used to find the growth rate. The sign of γ determines the stability of the pre-industrial state: positive values indicate instability and negative indicate stability.

The results of this experiment are plotted in Fig. 6. The figure shows the changing CO_2 levels for different values of ECS. CO_2 levels show exponential change over a millennial timescale. For large enough ECS values, there is exponential growth, indicating an unstable steady state, but for smaller values of ECS the system undergoes exponential decay, indicating a stable steady state. The growth rates, given by the slopes of these lines, are plotted in Fig. 7 against ECS.

Figure 7 shows the growth rates of atmospheric CO_2 as a function of ECS. The curve given by equation (12) was fitted to this data to enable estimation of the critical ECS value, which occurs when the growth rate is 0. The critical ECS value was found to be $10.9 \pm 0.6\mathrm{K}$, where the uncertainty is given by a 95% confidence interval. This compares remarkably well with the prediction of the simple model, with the central estimate matching its prediction.

This suggests that the simple model captures the relevant processes needed to determine the stability of the climate-carbon system.

4 Discussion and Conclusions

In this study, we have examined the conditions under which the climate-carbon state would be unstable. This was motivated, in part, by the fact that some CMIP6 ESMs exhibit high ECS values. To perform the assessment, we analysed a simple climate-

https://doi.org/10.5194/egusphere-2025-3703
Preprint. Discussion started: 18 August 2025

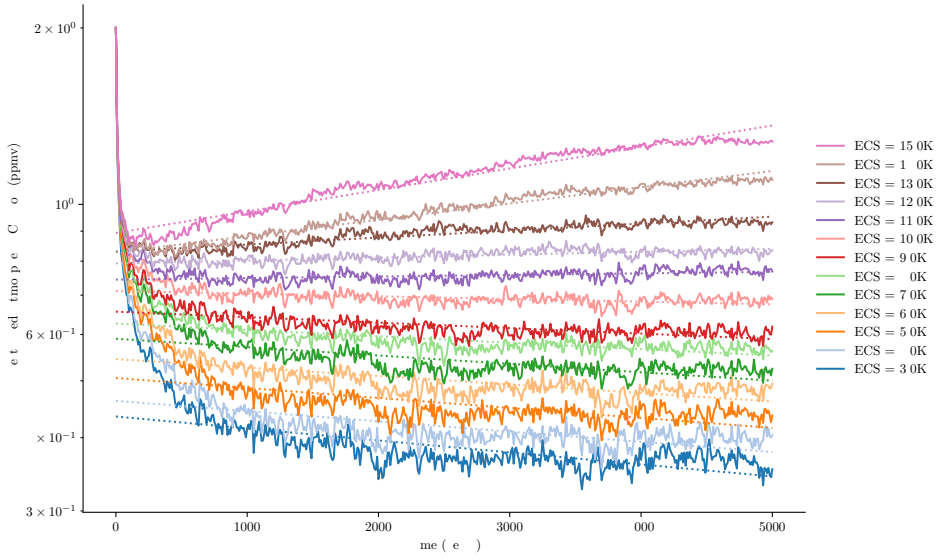

Figure 6. Atmospheric CO_2 from a JULES run for a variety of different climate sensitives. The system was initialised from an equilibrium state and given a perturbation of 2ppmv of CO_2. After an initial transient the atmospheric CO_2 changes exponentially with time, which corresponds to a linear change on a logarithmic scale. The dotted line is a fit to the exponential change phase and shows that as ECS increases, the system transitions from stable exponential decay to unstable exponential growth.

carbon model using linear stability theory. Additionally, we tested such predictions derived from such a simpler model against a more complex model for the land surface with atmospheric feedbacks, JULES/IMOGEN.

Using the simple model and the parameters presented in table 1, we were able to demonstrate that the pre-industrial climate-carbon state would be unstable for an ECS of greater than 10.9K, a finding that is also supported when using JULES/IMOGEN. This value is greater than the likely range of ECS based-on multiple observational constraints, of 2.6 – 3.9K (Sherwood et al., 2020). Our finding of this higher value of ECS at which the climate-carbon cycle system becomes unstable is to be expected given the observed stability of the system in its pre-industrial state. However, certain combinations of parameters lead to a critical ECS of under 6K suggesting that some ESMs may exhibit unrealistic unstable pre-industrial equilibria.

We have derived an approximate formula, equation (13), for the parameter values that lead to instability. This formula gives the factors that help keep the climate-carbon system stable. The important factors are CO_2 fertilisation of photosynthesis, the relative quantities of carbon in the atmosphere and in the land, and the ocean drawdown of carbon.

Nevertheless, the simple model has certain limitations. To keep the model tractable, spatial heterogeneity was ignored and we used a low dimensional representation of the dynamics of the climate-carbon system. More fundamentally, we neglected processes which could affect the system stability. The effect of changing temperature on terrestrial NPP is ignored, as is its effect on ocean uptake.

https://doi.org/10.5194/egusphere-2025-3703
Preprint. Discussion started: 18 August 2025

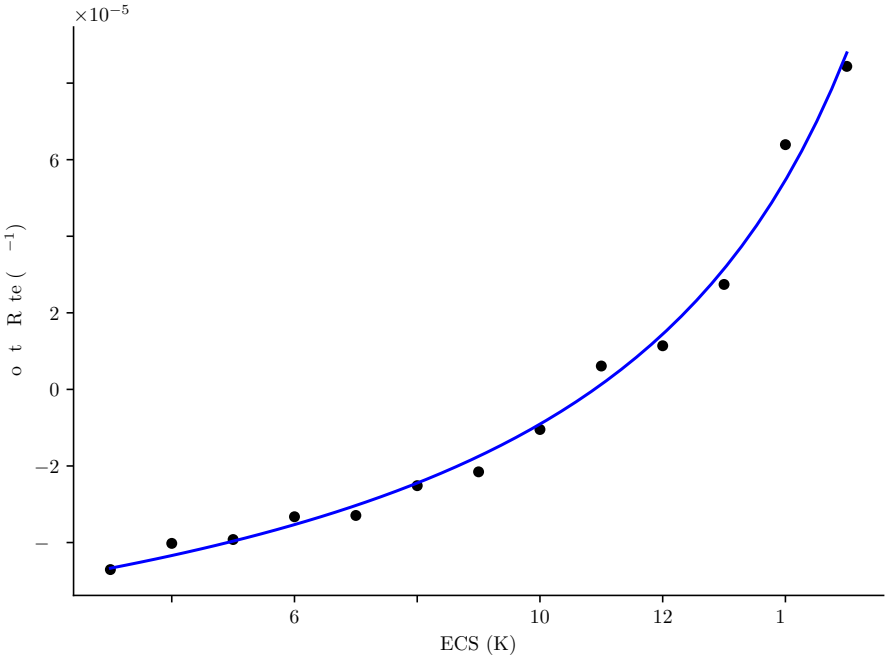

Figure 7. The growth rates of CO_2 as estimated from the time series shown in Fig. 6. Fitting equation (12) gives the blue line. The x-intercept gives the critical ECS at which the bifurcation occurs. The estimated critical ECS is 10.9 ± 0.6K.

Despite these problems, the simple model agrees with a more complex spatially resolved model, JULES, on the critical ECS that leads to an instability. This agreement gives confidence in the simple model's ability to give information about the bifurcation.

JULES/IMOGEN cannot be integrated for as long as the simple model can, so we are unable to verify if the simple model correctly predicts the dynamics of the system after the bifurcation. The simple model predicts that the system has a large amplitude limit cycle. This finding should be viewed with caution as the limit cycle visits regions of phase space (for example very high and low CO_2 concentrations) where the simple model's assumptions are no longer valid.

An interesting result of our stability analysis is the manner in which the stability of the state depends on the amount of carbon in the atmosphere. In particular, equation (13) suggests that the critical ECS scales with the ratio of atmospheric to land carbon stores. This effect was attributed to the linear dependence of respiration on land carbon and the logarithmic dependence of radiative forcing on atmospheric carbon. Importantly, this result suggests that as atmospheric carbon increases due to anthropogenic emissions, the climate-carbon system may become more not less stable. Conversely, climate-carbon states with lower atmospheric carbon, for example at the Last Glacial Maximum (LGM), are less stable. We estimate that a model with ECS greater than 4.5K and negligible CO_2 fertilization could suffer a climate-carbon cycle instability at LGM levels of CO_2, most likely manifested as a continual drift in the atmospheric CO_2 concentration.

https://doi.org/10.5194/egusphere-2025-3703
Preprint. Discussion started: 18 August 2025

These results also have implications for future coupled climate-carbon modelling. Although our critical ECS estimate of 10.9K is larger than the ECS values produced by ESMs, the critical ECS becomes comparable with the ECS values produced by ESMs if the strength of the CO_2 fertilisation effect is reduced. This means that if a model has a weak CO_2 fertilisation response, perhaps because of strong nitrogen limitations, the model may not have a stable pre-industrial state. As the real pre-industrial state was stable, this offers a potential way to test the realism of models.

In summary, we have examined the possibility of an instability within the climate-carbon system. This instability is caused by a positive feedback loop between global temperatures and heterotrophic respiration. We find that this instability can only occur for sufficiently high ECS. Our analysis suggests that the high ECS values of some ESMs combined with a weak CO_2 fertilisation effect may not be compatible with a stable glacial climate.

Code and data availability. Code and data used in this paper can be found at https://github.com/josephjclarke/Climate-Carbon-Instability. The JULES code used in these simulations is available from the Met Office Science Repository Service (registration required) at https://code.metoffice.gov.uk/trac/jules. The suite used is u-dr675 and available (registration required) at https://code.metoffice.gov.uk/trac/roses-u.

Author contributions. JC analysed the simple model and JULES runs as well as producing the figures. PDLR performed the continuation analysis. MS and RV helped parametrise the model. CH helped with performing long integrations with JULES/IMOGEN. PC conceptualised the study. All authors helped with interpreting the results and drafting the paper.

Competing interests. The authors declare no competing interests.

Acknowledgements. JC is grateful to Eleanor Burke for assistance with setting up JULES/IMOGEN. PDLR and PC acknowledge support from the European Union's Horizon Europe research and innovation programme under grant agreement No. 101137601 (ClimTip): Funded by the European Union. PDLR, PC, MW and CH acknowledge support from the UK Advanced Research and Invention Agency (ARIA) via the project 'AdvanTip'. JC, CH and PC acknowledge support from the PREDICT project which has received funding from the European Space Agency (ESA) under ESA Contract No. 4000146344/24/I-LR. RV acknowledges support from Schmidt Sciences through the CALIPSO project.

https://doi.org/10.5194/egusphere-2025-3703
Preprint. Discussion started: 18 August 2025

References

Arora, V. K., Katavouta, A., Williams, R. G., Jones, C. D., Brovkin, V., Friedlingstein, P., Schwinger, J., Bopp, L., Boucher, O., Cadule, P., Chamberlain, M. A., Christian, J. R., Delire, C., Fisher, R. A., Hajima, T., Ilyina, T., Joetzjer, E., Kawamiya, M., Koven, C. D., Krasting, J. P., Law, R. M., Lawrence, D. M., Lenton, A., Lindsay, K., Pongratz, J., Raddatz, T., Séférian, R., Tachiiri, K., Tjiputra, J. F., Wiltshire, A., Wu, T., and Ziehn, T.: Carbon-concentration and carbon-climate feedbacks in CMIP6 models and their comparison to CMIP5 models, Biogeosciences, 17, 4173–4222, https://doi.org/10.5194/bg-17-4173-2020, 2020.

Best, M. J., Pryor, M., Clark, D. B., Rooney, G. G., Essery, R. L. H., Ménard, C. B., Edwards, J. M., Hendry, M. A., Porson, A., Gedney, N., Mercado, L. M., Sitch, S., Blyth, E., Boucher, O., Cox, P. M., Grimmond, C. S. B., and Harding, R. J.: The Joint UK Land Environment Simulator (JULES), model description – Part 1: Energy and water fluxes, Geoscientific Model Development, 4, 677–699, https://doi.org/10.5194/gmd-4-677-2011, 2011.

Bolin, B. and Eriksson, E.: Distribution of matter in the sea and the atmosphere, The Atmosphere and the Sea in Motion, pp. 130–142, 1959.

Byrne, M. P. and O'Gorman, P. A.: Trends in continental temperature and humidity directly linked to ocean warming, Proceedings of the National Academy of Sciences, 115, 4863–4868, https://doi.org/10.1073/pnas.1722312115, 2018.

Canadell, J. G., Monteiro, P. M. S., Costa, M. H., da Cunha, L., Cox, P. M., Eliseev, A. V., Henson, S., Ishii, M., Jaccard, S., Koven, C., Lohila, A., Patra, P. K., Piao, S., Rogelj, J., Syampungani, S., Zaehle, S., and Zickfeld, K.: Global Carbon and Other Biogeochemical Cycles and Feedbacks, in: Climate Change 2021 – The Physical Science Basis, edited by Masson-Delmotte, V., Zhai, P., Pirani, A., Connors, S. L., Péan, C., Berger, S., Caud, N., Chen, Y., Goldfarb, L., Gomis, M. I., Huang, M., Leitzell, K., Lonnoy, E., Matthews, J. B. R., Maycock, T. K., Waterfield, T., Yelekçi, O., Yu, R., and Zhou, B., pp. 673–816, Cambridge University Press, Cambridge, UK and New York, NY, USA, https://doi.org/10.1017/9781009157896.007, section: 5, 2021.

Chen, D., Rojas, M., Samset, B., Cobb, K., Diongue Niang, A., Edwards, P., Emori, S., Faria, S., Hawkins, E., Hope, P., Huybrechts, P., Meinshausen, M., Mustafa, S., Plattner, G.-K., and Tréguier, A.-M.: Framing, context, and methods, in: Climate change 2021: The physical science basis. Contribution of working group I to the sixth assessment report of the intergovernmental panel on climate change, edited by Masson-Delmotte, V., Zhai, P., Pirani, A., Connors, S. L., Péan, C., Berger, S., Caud, N., Chen, Y., Goldfarb, L., Gomis, M. I., Huang, M., Leitzell, K., Lonnoy, E., Matthews, J. B. R., Maycock, T. K., Waterfield, T., Yelekçi, O., Yu, R., and Zhou, B., pp. 147–286, Cambridge University Press, Cambridge, UK and New York, NY, USA, https://doi.org/10.1017/9781009157896.003, section: 1 Type: Book Section, 2021.

Clark, D. B., Mercado, L. M., Sitch, S., Jones, C. D., Gedney, N., Best, M. J., Pryor, M., Rooney, G. G., Essery, R. L. H., Blyth, E., Boucher, O., Harding, R. J., Huntingford, C., and Cox, P. M.: The Joint UK Land Environment Simulator (JULES), model description – Part 2: Carbon fluxes and vegetation dynamics, Geoscientific Model Development, 4, 701–722, https://doi.org/10.5194/gmd-4-701-2011, 2011.

Cox, P. M., Betts, R. A., Jones, C. D., Spall, S. A., and Totterdell, I. J.: Acceleration of global warming due to carbon-cycle feedbacks in a coupled climate model, Nature, 408, 184–187, https://doi.org/10.1038/35041539, publisher: Nature Publishing Group, 2000.

Cox, P. M., Huntingford, C., and Jones, C. D.: Conditions for sink-to-source transitions and runaway feedbacks from the land carbon cycle, in: Avoiding Dangerous Climate Change, Cambridge University Press, ISBN 978-0-521-86471-8, https://ore.exeter.ac.uk/repository/handle/10036/48545, accepted: 2009-02-05T16:51:38Z, 2006.

Cummins, D. P., Stephenson, D. B., and Stott, P. A.: Optimal Estimation of Stochastic Energy Balance Model Parameters, Journal of Climate, 33, 7909–7926, https://doi.org/10.1175/JCLI-D-19-0589.1, 2020.

https://doi.org/10.5194/egusphere-2025-3703
Preprint. Discussion started: 18 August 2025

Davidson, E. A. and Janssens, I. A.: Temperature sensitivity of soil carbon decomposition and feedbacks to climate change, https://doi.org/10.1038/nature04514, iSSN: 00280836 Issue: 7081 Pages: 165–173 Publication Title: Nature Volume: 440, 2006.

DeVries, T.: The Ocean Carbon Cycle, Annual Review of Environment and Resources, 47, 317–341, https://doi.org/10.1146/annurev-environ-120920-111307, 2022.

Ermentrout, B.: Simulating, Analyzing, and Animating Dynamical Systems, Software, Environments, and Tools, Society for Industrial and Applied Mathematics, ISBN 978-0-89871-506-4, https://doi.org/10.1137/1.9780898718195, 2002.

Friedlingstein, P., Cox, P., Betts, R., Bopp, L., von Bloh, W., Brovkin, V., Cadule, P., Doney, S., Eby, M., Fung, I., Bala, G., John, J., Jones, C., Joos, F., Kato, T., Kawamiya, M., Knorr, W., Lindsay, K., Matthews, H. D., Raddatz, T., Rayner, P., Reick, C., Roeckner, E., Schnitzler, K.-G., Schnur, R., Strassmann, K., Weaver, A. J., Yoshikawa, C., and Zeng, N.: Climate–Carbon Cycle Feedback Analysis: Results from the C4MIP Model Intercomparison, Journal of Climate, 19, 3337–3353, https://doi.org/10.1175/JCLI3800.1, 2006.

Friedlingstein, P., Meinshausen, M., Arora, V. K., Jones, C. D., Anav, A., Liddicoat, S. K., and Knutti, R.: Uncertainties in CMIP5 Climate Projections due to Carbon Cycle Feedbacks, Journal of Climate, 27, 511–526, https://doi.org/10.1175/JCLI-D-12-00579.1, publisher: American Meteorological Society Section: Journal of Climate, 2014.

Friedlingstein, P., O'Sullivan, M., Jones, M. W., Andrew, R. M., Gregor, L., Hauck, J., Le Quéré, C., Luijkx, I. T., Olsen, A., Peters, G. P., Peters, W., Pongratz, J., Schwingshackl, C., Sitch, S., Canadell, J. G., Ciais, P., Jackson, R. B., Alin, S. R., Alkama, R., Arneth, A., Arora, V. K., Bates, N. R., Becker, M., Bellouin, N., Bittig, H. C., Bopp, L., Chevallier, F., Chini, L. P., Cronin, M., Evans, W., Falk, S., Feely, R. A., Gasser, T., Gehlen, M., Gkritzalis, T., Gloege, L., Grassi, G., Gruber, N., Gürses, O., Harris, I., Hefner, M., Houghton, R. A., Hurtt, G. C., Iida, Y., Ilyina, T., Jain, A. K., Jersild, A., Kadono, K., Kato, E., Kennedy, D., Klein Goldewijk, K., Knauer, J., Korsbakken, J. I., Landschützer, P., Lefèvre, N., Lindsay, K., Liu, J., Liu, Z., Marland, G., Mayot, N., McGrath, M. J., Metzl, N., Monacci, N. M., Munro, D. R., Nakaoka, S.-I., Niwa, Y., O'Brien, K., Ono, T., Palmer, P. I., Pan, N., Pierrot, D., Pocock, K., Poulter, B., Resplandy, L., Robertson, E., Rödenbeck, C., Rodriguez, C., Rosan, T. M., Schwinger, J., Séférian, R., Shutler, J. D., Skjelvan, I., Steinhoff, T., Sun, Q., Sutton, A. J., Sweeney, C., Takao, S., Tanhua, T., Tans, P. P., Tian, X., Tian, H., Tilbrook, B., Tsujino, H., Tubiello, F., van der Werf, G. R., Walker, A. P., Wanninkhof, R., Whitehead, C., Willstrand Wranne, A., Wright, R., Yuan, W., Yue, C., Yue, X., Zaehle, S., Zeng, J., and Zheng, B.: Global Carbon Budget 2022, Earth System Science Data, 14, 4811–4900, https://doi.org/10.5194/essd-14-4811-2022, 2022.

Geoffroy, O., Saint-Martin, D., Olivié, D. J. L., Voldoire, A., Bellon, G., and Tytéca, S.: Transient Climate Response in a Two-Layer Energy-Balance Model. Part I: Analytical Solution and Parameter Calibration Using CMIP5 AOGCM Experiments, Journal of Climate, 26, 1841–1857, https://doi.org/10.1175/JCLI-D-12-00195.1, 2013.

Glotter, M. J., Pierrehumbert, R. T., Elliott, J. W., Matteson, N. J., and Moyer, E. J.: A simple carbon cycle representation for economic and policy analyses, Climatic Change, 126, 319–335, https://doi.org/10.1007/s10584-014-1224-y, 2014.

Huntingford, C. and Mercado, L. M.: High chance that current atmospheric greenhouse concentrations commit to warmings greater than 1.5 °C over land, Scientific Reports, 6, 30 294, https://doi.org/10.1038/srep30294, 2016.

Huntingford, C., Cox, P. M., and Lenton, T. M.: Contrasting responses of a simple terrestrial ecosystem model to global change, Ecological Modelling, 134, 41–58, https://doi.org/10.1016/S0304-3800(00)00330-6, publisher: Elsevier, 2000.

Huntingford, C., Booth, B. B. B., Sitch, S., Gedney, N., Lowe, J. A., Liddicoat, S. K., Mercado, L. M., Best, M. J., Weedon, G. P., Fisher, R. A., Lomas, M. R., Good, P., Zelazowski, P., Everitt, A. C., Spessa, A. C., and Jones, C. D.: IMOGEN: an intermediate complexity model to evaluate terrestrial impacts of a changing climate, Geoscientific Model Development, 3, 679–687, https://doi.org/10.5194/gmd-3-679-2010, 2010.

https://doi.org/10.5194/egusphere-2025-3703
Preprint. Discussion started: 18 August 2025

Jenkinson, D. S., Adams, D. E., and Wild, A.: Model estimates of CO2 emissions from soil in response to global warming, Nature, 351, 1991.

Jones, C. D. and Cox, P.: Constraints on the temperature sensitivity of global soil respiration from the observed interannual variability in atmospheric CO2, Atmospheric Science Letters, 2, 166–172, https://doi.org/10.1006/asle.2001.0041, 2001.

Jones, C. D., Hughes, J. K., Bellouin, N., Hardiman, S. C., Jones, G. S., Knight, J., Liddicoat, S., O'Connor, F. M., Andres, R. J., Bell, C., Boo, K.-O., Bozzo, A., Butchart, N., Cadule, P., Corbin, K. D., Doutriaux-Boucher, M., Friedlingstein, P., Gornall, J., Gray, L., Halloran, P. R., Hurtt, G., Ingram, W. J., Lamarque, J.-F., Law, R. M., Meinshausen, M., Osprey, S., Palin, E. J., Parsons Chini, L., Raddatz, T., Sanderson, M. G., Sellar, A. A., Schurer, A., Valdes, P., Wood, N., Woodward, S., Yoshioka, M., and Zerroukat, M.: The HadGEM2-ES implementation of CMIP5 centennial simulations, Geoscientific Model Development, 4, 543–570, https://doi.org/10.5194/gmd-4-543-2011, publisher: Copernicus GmbH, 2011.

Joos, F., Bruno, M., Fink, R., Siegenthaler, U., Stocker, T. F., Le Quéré, C., and Sarmiento, J. L.: An efficient and accurate representation of complex oceanic and biospheric models of anthropogenic carbon uptake, Tellus B: Chemical and Physical Meteorology, 48, 397, https://doi.org/10.3402/tellusb.v48i3.15921, 1996.

Judd, E. J., Tierney, J. E., Lunt, D. J., Montañez, I. P., Huber, B. T., Wing, S. L., and Valdes, P. J.: A 485-million-year history of Earth's surface temperature, Science, 385, https://doi.org/10.1126/science.adk3705, publisher: American Association for the Advancement of Science, 2024.

Kageyama, M., Albani, S., Braconnot, P., Harrison, S. P., Hopcroft, P. O., Ivanovic, R. F., Lambert, F., Marti, O., Peltier, W. R., Peterschmitt, J.-Y., Roche, D. M., Tarasov, L., Zhang, X., Brady, E. C., Haywood, A. M., LeGrande, A. N., Lunt, D. J., Mahowald, N. M., Mikolajewicz, U., Nisancioglu, K. H., Otto-Bliesner, B. L., Renssen, H., Tomas, R. A., Zhang, Q., Abe-Ouchi, A., Bartlein, P. J., Cao, J., Li, Q., Lohmann, G., Ohgaito, R., Shi, X., Volodin, E., Yoshida, K., Zhang, X., and Zheng, W.: The PMIP4 contribution to CMIP6 – Part 4: Scientific objectives and experimental design of the PMIP4-CMIP6 Last Glacial Maximum experiments and PMIP4 sensitivity experiments, Geoscientific Model Development, 10, 4035–4055, https://doi.org/10.5194/gmd-10-4035-2017, publisher: Copernicus GmbH, 2017.

Marcott, S. A., Bauska, T. K., Buizert, C., Steig, E. J., Rosen, J. L., Cuffey, K. M., Fudge, T. J., Severinghaus, J. P., Ahn, J., Kalk, M. L., McConnell, J. R., Sowers, T., Taylor, K. C., White, J. W. C., and Brook, E. J.: Centennial-scale changes in the global carbon cycle during the last deglaciation, Nature, 514, 616–619, https://doi.org/10.1038/nature13799, publisher: Nature Publishing Group, 2014.

Myhre, G., Highwood, E. J., Shine, K. P., and Stordal, F.: New estimates of radiative forcing due to well mixed greenhouse gases, Geophysical Research Letters, 25, 2715–2718, https://doi.org/10.1029/98GL01908, 1998.

Petit, J. R., Jouzel, J., Raynaud, D., Barkov, N. I., Barnola, J.-M., Basile, I., Bender, M., Chappellaz, J., Davis, M., Delaygue, G., Delmotte, M., Kotlyakov, V. M., Legrand, M., Lipenkov, V. Y., Lorius, C., PÉpin, L., Ritz, C., Saltzman, E., and Stievenard, M.: Climate and atmospheric history of the past 420,000 years from the Vostok ice core, Antarctica, Nature, 399, 429–436, https://doi.org/10.1038/20859, publisher: Nature Publishing Group, 1999.

Schimel, D., Stephens, B. B., and Fisher, J. B.: Effect of increasing CO2 on the terrestrial carbon cycle, Proceedings of the National Academy of Sciences, 112, 436–441, https://doi.org/10.1073/pnas.1407302112, publisher: Proceedings of the National Academy of Sciences, 2015.

Sherwood, S. C., Webb, M. J., Annan, J. D., Armour, K. C., Forster, P. M., Hargreaves, J. C., Hegerl, G., Klein, S. A., Marvel, K. D., Rohling, E. J., Watanabe, M., Andrews, T., Braconnot, P., Bretherton, C. S., Foster, G. L., Hausfather, Z., von der Heydt, A. S., Knutti, R., Mauritsen, T., Norris, J. R., Proistosescu, C., Rugenstein, M., Schmidt, G. A., Tokarska, K. B., and Zelinka, M. D.: An Assessment of Earth's Climate Sensitivity Using Multiple Lines of Evidence, Reviews of Geophysics, 58, https://doi.org/10.1029/2019RG000678, 2020.

https://doi.org/10.5194/egusphere-2025-3703
Preprint. Discussion started: 18 August 2025

Varney, R. M., Chadburn, S. E., Burke, E. J., Jones, S., Wiltshire, A. J., and Cox, P. M.: Simulated responses of soil carbon to climate change in CMIP6 Earth system models: the role of false priming, Biogeosciences, 20, 3767–3790, https://doi.org/10.5194/bg-20-3767-2023, publisher: Copernicus GmbH, 2023.

Williamson, M. S., Cox, P. M., Huntingford, C., and Nijsse, F. J. M. M.: Testing the assumptions in emergent constraints: why does the "emergent constraint on equilibrium climate sensitivity from global temperature variability" work for CMIP5 and not CMIP6?, Earth System Dynamics, 15, 829–852, https://doi.org/10.5194/esd-15-829-2024, 2024.

Zachos, J., Pagani, M., Sloan, L., Thomas, E., and Billups, K.: Trends, Rhythms, and Aberrations in Global Climate 65 Ma to Present, Science, 292, 686–693, https://doi.org/10.1126/science.1059412, publisher: American Association for the Advancement of Science, 2001.

Zelinka, M. D., Myers, T. A., McCoy, D. T., Po-Chedley, S., Caldwell, P. M., Ceppi, P., Klein, S. A., and Taylor, K. E.: Causes of Higher Climate Sensitivity in CMIP6 Models, Geophysical Research Letters, 47, 1–12, https://doi.org/10.1029/2019GL085782, 2020.